Acta Materia Medica

Research Article

The direct STAT3 inhibitor 6-ethoxydihydrosanguinarine exhibits anticancer activity in gastric cancer

Graphical abstract

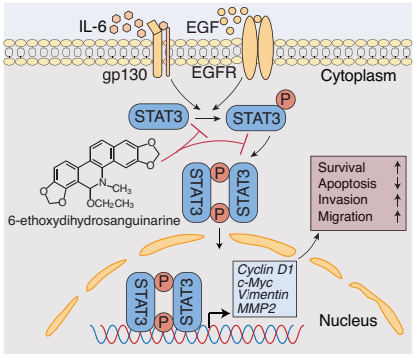

Highlights

- 6-ethoxydihydrosanguinarine suppresses survival and invasive behavior of gastric cancer cells.
- 6-ethoxydihydrosanguinarine inhibits the activity of STAT3 to suppress the survival and invasive behavior of gastric cancer cells.
- 6-ethoxydihydrosanguinarine inhibits the binding of phosphorylated and non-phosphorylated STAT3 to target DNA.
- 6-ethoxydihydrosanguinarine binds directly to the SH2 domain of STAT3.

Authors

Xuewen Liu, Xin Jin, Hongling Ou, Chen Qian, Hui Wu, Chunmei Zuo, Yuliang Ren, Miaoxin Fu, Te Zhang, Liang Zhang, Yuan Si, Ying Liu

Correspondence

ying_liu1002@163.com (Y. Liu); siyuan138@126.com (Y. Si)

In brief

As a novel STAT3 inhibitor, 6-ethoxydihydrosanguinarine inhibits the malignant progression of gastric cancer mainly by directly binding to the SH2 domain of STAT3.

https://doi.org/10.15212/amm-2022-0027
Acta Materia Medica 2022, Volume 1, Issue 3, p. 365-380

Acta Materia Medica

Research Article

The direct STAT3 inhibitor 6-ethoxydihydrosanguinarine exhibits anticancer activity in gastric cancer

Xuewen Liu[a,b,c,d,1], Xin Jin[a,c,1], Hongling Ou[a,c], Chen Qian[a,c], Hui Wu[a,c], Chunmei Zuo[a,c], Yuliang Ren[a,c,d], Miaoxin Fu[a,c,d], Te Zhang[a,b,d], Liang Zhang[a,c,d], Yuan Si[a,c,d,*], Ying Liu[a,b,c,d,*]

[a]Laboratory of Molecular Target Therapy of Cancer, Institute of Basic Medical Sciences, Hubei University of Medicine, Shiyan, Hubei, China
[b]Hubei Key Laboratory of Wudang Local Chinese Medicine Research, Hubei University of Medicine, Shiyan, Hubei, China
[c]Hubei Key Laboratory of Embryonic Stem Cell Research, Hubei University of Medicine, Shiyan, Hubei, China
[d]Laboratory of Molecular Target Therapy of Cancer, Biomedical Research Institute, Hubei University of Medicine, Shiyan, Hubei, China

[1]These authors contributed equally to this work.

***Correspondence:** ying_liu1002@163.com (Y. Liu); siyuan138@126.com (Y. Si)

Received: 10 August 2022; Revised: 14 September 2022; Accepted: 16 September 2022

Published online: 6 October 2022

DOI 10.15212/AMM-2022-0027

ABSTRACT

Signal transducer and activator of transcription 3 (STAT3) plays a key role in promoting tumor malignant progression. Suppression of hyperactivated STAT3 signaling has emerged as a potential therapeutic strategy for many cancer types. In this study, the effect of 6-ethoxydihydrosanguinarine (6-EDS), a secondary transformation product formed from dihydrosanguinarine, isolated from *Macleaya* (Papaveraceae), was evaluated in gastric cancer (GC). We demonstrated that 6-EDS inhibited the survival, migration, and invasiveness of GC cells *in vitro*. Moreover, 6-EDS inhibited STAT3 phosphorylation and transcriptional activity, thus suppressing the mRNA expression of downstream target genes associated with the malignant survival, migration, and invasiveness of GC cells. Molecular docking indicated that 6-EDS directly bound the SH2 domain of STAT3. Molecular dynamics simulations suggested that 6-EDS inhibited the binding of phosphorylated and non-phosphorylated STAT3 to target DNA. Cellular thermal-shift assays and microscale thermophoresis further confirmed the direct binding of 6-EDS to STAT3. Site-directed mutagenesis indicated that the S611 residue in the SH2 domain of STAT3 is critical for 6-EDS binding. *In vivo*, 6-EDS decreased tumor growth in xenografted nude mice by blocking STAT3 signaling. These findings indicated that 6-EDS, a direct STAT3 inhibitor, may be a potent anticancer candidate for GC therapy.

Keywords: 6-ethoxydihydrosanguinarine, gastric cancer, STAT3, invasion, migration

1. INTRODUCTION

Gastric cancer (GC), a common malignancy of the alimentary system, is the third leading cause of tumor-associated death worldwide [1]. It has the highest annual incidence in East Asian countries compared to other regions in Asia [2]. Approximately 679,000 patients are newly diagnosed with GC in China each year. Owing to its large population, China accounts for most patients with GC in East Asia [3]. Despite the substantial improvements made in surgical techniques and medications for GC over the past decade, the 5-year survival rate for patients with advanced GC is poor, at <15% [4]. Identifying new drugs remains the main strategy for exploring new treatment options for tumors, including GC.

Signal transducers and activators of transcription (STAT) is a family of nucleocytoplasmic shuttling transcription factors responsible for the signal transduction of extracellular cytokines and the activation of gene transcription [5]. This family includes STAT1, STAT2, STAT3, STAT4, STAT5a, STAT5b, and STAT6, which have relatively conserved homologous functional domains. All seven STAT proteins play central roles in cellular immune responses, cell survival, differentiation, angiogenesis, and motility [6]. STAT3 is the most widely studied member of the STAT family, and the most closely associated with tumorigenesis; it is a key regulatory molecule in various oncogenic signaling pathways [7]. Abnormally activated STAT3 is present in more than 70% of human cancers [8, 9], including breast, lung,

liver, stomach, brain, colon, cervix, and prostate cancers, and acute myeloid leukemia and multiple myeloma [7]. The protein structure of STAT3 contains an N-terminal domain, a coiled-coil domain, a DNA-binding domain, a linker region, an SH2 domain, and a C-terminal transactivation domain, similarly to other STAT family members [10]. STAT3 exists as an inactive monomer in the cytoplasm. After the tyrosine residues of JAKs are phosphorylated by upstream growth factor receptors (e.g., gp130 and EGFR), the SH2 domain of STAT3 recognizes and binds these phosphorylated-tyrosine docking sites, thus placing STAT3 in proximity to activated JAKs; phosphorylation then occurs at Y705 in the C-terminal transactivation domain. Phosphorylation of Y705 promotes SH2 domain-mediated head-to-tail dimerization of STAT3 followed by translocation to the nucleus. After entry into the nucleus, STAT3 binds cognate response elements in target gene promoters, thereby regulating the expression of regulatory transcription factors promoting cell growth (such as cyclin D1), survival (such as survivin), and cell invasion and migration (such as MMP proteins and vimentin) [11]. In addition, studies increasingly indicate that constitutive activation of STAT3 promotes tumor-induced immune suppression at several levels [12]. Given the above characteristics, STAT3 has been widely studied in tumor malignant progression and as a tumor target.

The herbaceous perennial *Macleaya cordata* (Wild.) R. Br. belongs to the *Papaveraceae* family and is ubiquitously found in China, North America, and Europe [13, 14]. *M. cordata* is recorded in many ancient books as a traditional Chinese medicine. In recent years, studies have reported that it has a variety of pharmacological activities, such as antifungal, antimicrobial, anti-inflammatory, antioxidant, and antitumor activities [15–17]. Pharmacological studies have shown that the main biologically active ingredient of *M. cordata* is alkaloids. To date, 147 alkaloids have been identified and/or isolated in *M. cordata*. Most are isoquinoline alkaloids, including sanguinarine, chelidonine, allocryptine, dihydrochelerythrine, oxysanguinarine, and dihydrosanguinarine [18, 19]. The compound 6-ethoxydihydrosanguinarine (6-EDS, **Figure 1a**) is a secondary transformation product formed after dihydrosanguinarine is extracted from *M. cordata* [20]. Because the effect and mechanism of 6-EDS in GC was unclear, herein, we investigated the effects of 6-EDS in GC.

2. MATERIALS AND METHODS

2.1 Reagents

The compound 6-EDS, with a purity of ≥ 98%, was purchased from BioBioPha Co., Ltd. (Kunming, China).

2.2 Cell culture

Human GC cell lines BGC823, MGC803, and AGS were purchased from the ATCC, and were maintained in Dulbecco's modified Eagle's medium (Gibco, USA) supplemented with 10% FBS and antibiotics, and incubated in a humidified atmosphere with 5% CO_2 at 37°C.

2.3 Cell cytotoxicity assays

Cell cytotoxicity was determined with MTT assays and xCELLigence real time cell analysis (RTCA) assays. For MTT assays, cells were seeded into 96-well plates, then treated with 6-EDS. The absorbance was determined at 490 nm with an automated microplate reader (BioTek, USA) [21]. For RTCA assays, the cells were seeded into 16-well E-Plates (ACEA Biosciences, USA), and an xCELLigence RTCA HT Instrument (ACEA Biosciences, USA) was used for label-free, real-time, automated monitoring. After 24 h, the cells were treated with 6-EDS. The cell index analysis (15 min interval detection) lasted for 60 h.

2.4 Soft-agar colony-formation assays

Soft-agar colony-formation analysis was performed as previously described [22].

2.5 High-content analysis

The Operetta CLS™ high-content analysis system (PerkinElmer, Germany) was used to monitor the movement potential of cells. Cell tracks were recorded in real time to dynamically determine the migration. Cells were seeded into 96-well plates, and cell movement was recorded overnight in real time. The paths of the cells were automatically analyzed in Harmony 4.1 software.

2.6 Annexin V/PI double staining and apoptosis detection

Cells were incubated with 6-EDS for 24 h. Cell apoptosis was detected through annexin V/PI detection with an annexin V/PI kit (Dojindo, Japan). Flow cytometry was performed with a flow cytometer (Beckman, USA) [23].

2.7 Mitochondrial membrane potential measurement

After incubation with 6-EDS for 24 h, cells were collected and stained with the JC-1 fluorescent probe. After incubation for 20 min, a flow cytometer (Beckman, USA) was used to detect fluorescence.

2.8 DAPI staining

For observation of nuclear morphology, cells were fixed and then stained with DAPI (Beyotime, China). The images of stained cells were obtained with a fluorescence microscope (Olympus, Japan).

2.9 Western blotting

Western blotting was conducted according to the standard method described previously [24]. The primary antibodies used were anti-GAPDH, anti-MMP9, anti-cyclin D1, anti-JAK2 (Santa Cruz Biotechnology, USA); anti-phospho-STAT3 (Y705), anti-phospho-STAT3 (S727), anti-STAT3, anti-phospho-JAK2 (Y1007/Y1008), anti-E-cadherin, anti-caspase-9, anti-PARP, anti-caspase-3,

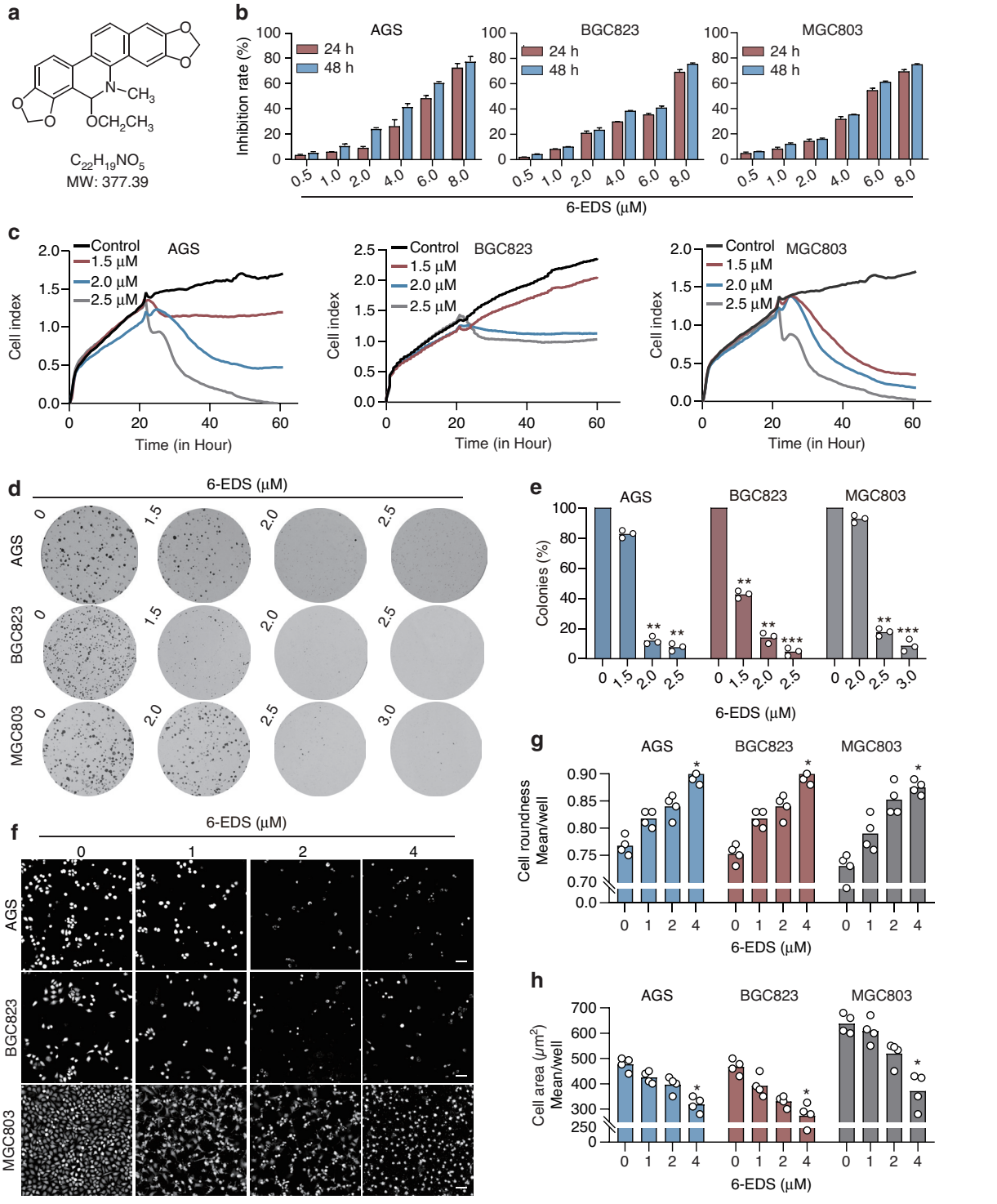

Figure 1 | The compound 6-EDS suppresses the growth of GC cells.
(a) Chemical structure of 6-EDS. (b) The inhibitory effects of 6-EDS on AGS, BGC823, and MGC803 cells, evaluated with MTT assays. (c) The inhibitory effects of 6-EDS on the viability of AGS, BGC823, and MGC803 cells, monitored with RTCA assays. (d, e) Colony-formation assays of AGS, BGC823, and MGC803 cells treated with 6-EDS. (f–h) AGS, BGC823, and MGC803 cells were treated with 6-EDS for 24 h. Growth of cells was assessed and imaged at 24 h through brightfield and digital phase-contrast microscopy with a Perkin-Elmer Operetta microscope (f). The roundness and area of AGS, BGC823, and MGC803 cells, determined at 24 h with Harmony software (g, h). Scale bars, 50 μm. $^*P < 0.05$, $^{**}P < 0.01$, $^{***}P < 0.001$.

Acta Materia Medica

anti-PARP, anti-phospho-EGFR (T1068), anti-EGFR (Cell Signaling Technology, USA); and anti-c-Myc, anti-MMP2, anti-vimentin, anti-Lamin B1 (Proteintech Group, USA).

2.10 Wound-healing assays

Wound-healing assays were performed as previously described [25]. ImageJ software was used for measuring the wound gaps.

2.11 xCELLigence real-time cellular analysis assay for cell invasion

The upper chamber of a 16-well CIM-Plate (ACEA Biosciences, USA) was pre-coated with 1 mg/mL Matrigel (BD Biosciences, USA) for 4 h. Cells (8×10^3 cells per well) in serum-free medium were seeded in the upper chambers, and complete medium containing 20% FBS was added to the lower chambers. Subsequently, an RTCA DPlus Instrument (ACEA Biosciences, USA) was used to detect the cell index (15-minute interval detection) for 50 h.

2.12 Invasion assays

Transwell invasion assays were performed as previously described [25].

2.13 Real-time quantitative PCR

Real-time quantitative PCR (qPCR) was performed on an ABI StepOnePlus™ Real-Time PCR System (ABI, USA) with SYBR® Green Real-time PCR Master Mix (Toyobo Co., Ltd., Japan). Primers are listed in **Table 1**.

2.14 Isolation of nuclear and cytoplasmic fractions

Nuclear and cytosolic fractions were separated with a Nuclear and Cytoplasmic Protein Extraction Kit (Beyotime Biotechnology, China). Western blotting was used to detect the expression of STAT3, Lamin B1, and GAPDH.

Table 1 | Primer sequences for qPCR.

Gene	Primer sequence
MMP2	F: ACGACCGCGACAAGAAGTAT
	R: ATTTGTTGCCCAGGAAAGTG
Vimentin	F: ACTACGTCCACCCGCACCTA
	R: CAGCGAGAAGTCCACCGAGT
Cyclin D1	F: GTCGCTGGAGCCCGTGA
	R: GGATGGAGTTGTCGGTGTAGATG
c-Myc	F: GGCTCCTGGCAAAAGGTCA
	R: CTGCGTAGTTGTGCTGATGT

F, forward; R, reverse.

2.15 Immunofluorescence assays

Cell or tissue sections were fixed in 4% formaldehyde, then blocked with 3% BSA/0.2% Triton X-100 in PBS. Subsequently, cells were incubated with antibody to STAT3, then with Alexa Fluor® 488-conjugated secondary antibody (Abbkine, China). Next, the slides were stained with DAPI (Beyotime Biotechnology, China). Fluorescence images were acquired on an Olympus laser scanning confocal microscope.

2.16 Transfection of DNA

The pcDNA3.1-EGFP-STAT3-Myc expression plasmid was purchased from HeBio Co. Ltd. (Shanghai, China). Plasmids were transfected with Lipofectamine® 3000 transfection reagent (Invitrogen, USA).

2.17 Molecular docking

The structure of the phosphorylated STAT3 core protein bound to DNA was obtained from the RCSB PDB database (PDB ID: 6NJS). Wild-type STAT3 was obtained by back-mutation to unphosphorylated tyrosine with the mutagenesis model in PyMOL. The missing DNA strands were repaired by base-pairing and modeled with the 3DNA webserver [26]. Then the structure was prepared by removal of hydrogen assignments at pH 7.0 with academic Maestro [27]. Water molecules near small-molecule-binding pockets were retained. Ligand-protein docking experiments were conducted mainly with Autodock Vina. The search space at the binding pocket was a rectangle of 22.5 Å × 22.5 Å × 22.5 Å in the X, Y, and Z dimensions. The docked poses were clustered with a tolerance of 2 Å root-mean-square deviations and were evaluated for the final docking structure according to the docking score.

2.18 Molecular dynamic simulation

Molecular dynamics (MD) simulations were performed with the GROMACS 5.1.5 program [28]. We constructed four systems to estimate the effects of 6-EDS on STAT3-DNA binding: (i) wild-type STAT3 with DNA (wt-STAT3_DNA), (ii) 6-EDS compound with wild-type STAT3 and DNA (6-EDS_wt-STAT3_DNA), (iii) 6-EDS with phosphorylated STAT3 (6-EDS_Y2P-STAT3), and (iv) 6-EDS with phosphorylated STAT3 and DNA (6-EDS_Y2P-STAT3_DNA). Every simulation system was solved with TIP3P waters and neutralization by Na^+ and Cl^- ions. The periodic boundary conditions had a minimal distance of 1.0 Å between the molecules and the edge of the box. [29]. The ff99SB force field was used for STAT3 and DNA, and the GAFF force field was used for 6-EDS topology [30]. Simulation systems were subjected to constant number of particles, volume, and temperature (NVT) equilibration, and constant number of particles, pressure, and temperature (NPT) equilibration. Finally, MD was performed for a period of 50 ns with 2-fs steps. The trajectory information was collected every 2 ps [31].

2.19 Binding-free-energy calculation

The binding free energies (ΔG_{bind}) were calculated with the MM/GBSA model [32]. The GROMACS output trajectory was correctly fitted, and PBC conditions were removed before the calculations were run with gmx_MMPBSA. ΔGbind was calculated as follows:

$$\Delta G_{bind} = \Delta H - T\Delta S \approx \Delta G_{solv} + \Delta G_{GAS} - T\Delta S \quad (1)$$

$$\Delta G_{GAS} = \Delta E_{int} + \Delta E_{vdw} + \Delta E_{ele} \quad (2)$$

$$\Delta G_{solv} = \Delta E_{SURF} + \Delta E_{GB} \quad (3)$$

Here, ΔG_{solv} refers to solvation free energy; ΔG_{GAS} refers to the gas-phase energy; TΔS refers to changes in the conformational entropy upon binding; and ΔE_{int} refers to the bond, angle, and dihedral energies, which were usually taken as zero. ΔE_{ele} refers to electrostatic; ΔE_{vdw} refers to van der Waals energies; and ΔG_{solv} refers to the sum of the no-electrostatic-solvation component (nonpolar contribution, e.g., ΔE_{SURF}) and the electrostatic solvation energy (polar contribution, e.g., ΔG_{PB}). TΔS was also omitted in this method, owing to its intrinsically low prediction accuracy [33, 34].

2.20 Microscale thermophoresis assays

Purified human STAT3 protein was labeled with a Monolith™ NT.115 Protein Labeling Kit (NanoTemper Technologies GmbH, Germany). Cells transfected with EGFP-STAT3 expression plasmid were lysed in RIPA buffer to isolate total protein. Subsequently, 16 serial dilutions of 6-EDS were prepared, ranging from 1.25 mM to 0.038 μM. The labeled STAT3 or cell lysates containing EGFP-STAT3 protein were quantified, then incubated with 6-EDS for 10 min in the dark. Samples were loaded into standard capillaries in the NanoTemper Monolith™ NT (NanoTemper Technologies GmbH, Germany). The dissociation constant (K_d) was then calculated.

2.21 Drug-affinity-responsive-target stability assays

Cells were harvested and lysed with lysis buffer (Sigma, USA). Lysates were treated with 6-EDS and then incubated with pronase (Sigma, USA) at 37°C for 30 min. The hydrolyzation of STAT3 was detected by western blotting [35].

2.22 Cellular thermal-shift assays

Cells were harvested and lysed with lysis buffer (Sigma, USA). Lysates were then heated at 35–55°C after incubation with 6-EDS for 30 min. The stabilizing effect of 6-EDS on STAT3 was detected by western blotting.

2.23 Xenograft experiments

Female nude mice 5–7 weeks old were purchased from Vital River Laboratory (Beijing, China) and monitored in an SPF environment. The mice were injected subcutaneously with 6×10^6 BGC823 cells. Before treatment, mice were randomly divided into two groups: a vehicle group (0.8% DMSO, 12% cremophor, and 8% ethanol in saline; n=7) and 6-EDS-treated group (intraperitoneal injection of 2.0 mg/kg 6-EDS; n=7). The mice were treated four times per week for a total of 4 weeks. Caliper measurements were performed twice per week with the following formula: $4\pi/3 \times (\text{width}/2)^2 \times (\text{length}/2)$. Mice were sacrificed when their tumors reached 1.5 cm, or they appeared moribund. Subcutaneous tumors were excised for western blotting, or were fixed and then embedded in paraffin for H&E staining and immunohistochemistry.

2.24 Statistical analysis

All experiments were repeated at least three times, and the data are presented as mean ± SD. Differences between data groups were evaluated for significance with Student's t-test for unpaired data or one-way analysis of variance and Bonferroni post-test. $P < 0.05$ indicates statistical significance.

3. RESULTS

3.1 6-EDS suppresses the growth of GC cells

We investigated the effects of 6-EDS on GC cell lines. The IC_{50} values of 6-EDS in AGS, BGC823, and MGC803 cells were 5.86 μM, 6.43 μM, and 5.48 μM, respectively, at 24 h (**Figure 1b**). We performed RTCA assays to monitor the proliferation ability of cells. The RTCA assays indicated that 6-EDS decreased the growth rates of AGS, BGC823, and MGC803 cells (**Figure 1c**). Next, colony-formation assays demonstrated that 6-EDS markedly decreased the clonogenic ability of AGS, BGC823, and MGC803 cells (**Figure 1d**). High-content imaging technology was used to track the morphology of cells. The number of tracked cells decreased after treatment with 6-EDS, and the mean roundness of cells treated with 6-EDS had increased at 24 h (**Figure 1h**, **1i**).

3.2 Mitochondrially mediated apoptosis is induced by 6-EDS in GC cells

Apoptosis was further analyzed in AGS, BGC823, and MGC803 cells. Annexin V/PI staining and flow cytometry assays showed that 6-EDS induced apoptosis of AGS, BGC823, and MGC803 cells (**Figure 2a**). DAPI staining further confirmed that 6-EDS induced chromatin condensation and fragmentation in AGS, BGC823, and MGC803 cells (**Figure 2b**). Next, the mitochondrial membrane potential (MMP) was measured. The red JC-1 aggregates indicated intact MMP, whereas green JC-1 monomers indicated damaged MMP. Fluorescence detection showed that 6-EDS treatment decreased the number of red fluorescent cells and increased the number of green fluorescent cells. Therefore, the ratio of red/green JC-1 fluorescence decreased (**Figure 2c**), thus suggesting that 6-EDS induced MMP damage in GC cells. Furthermore, expression of caspase and apoptotic protein was

Acta
Materia
Medica

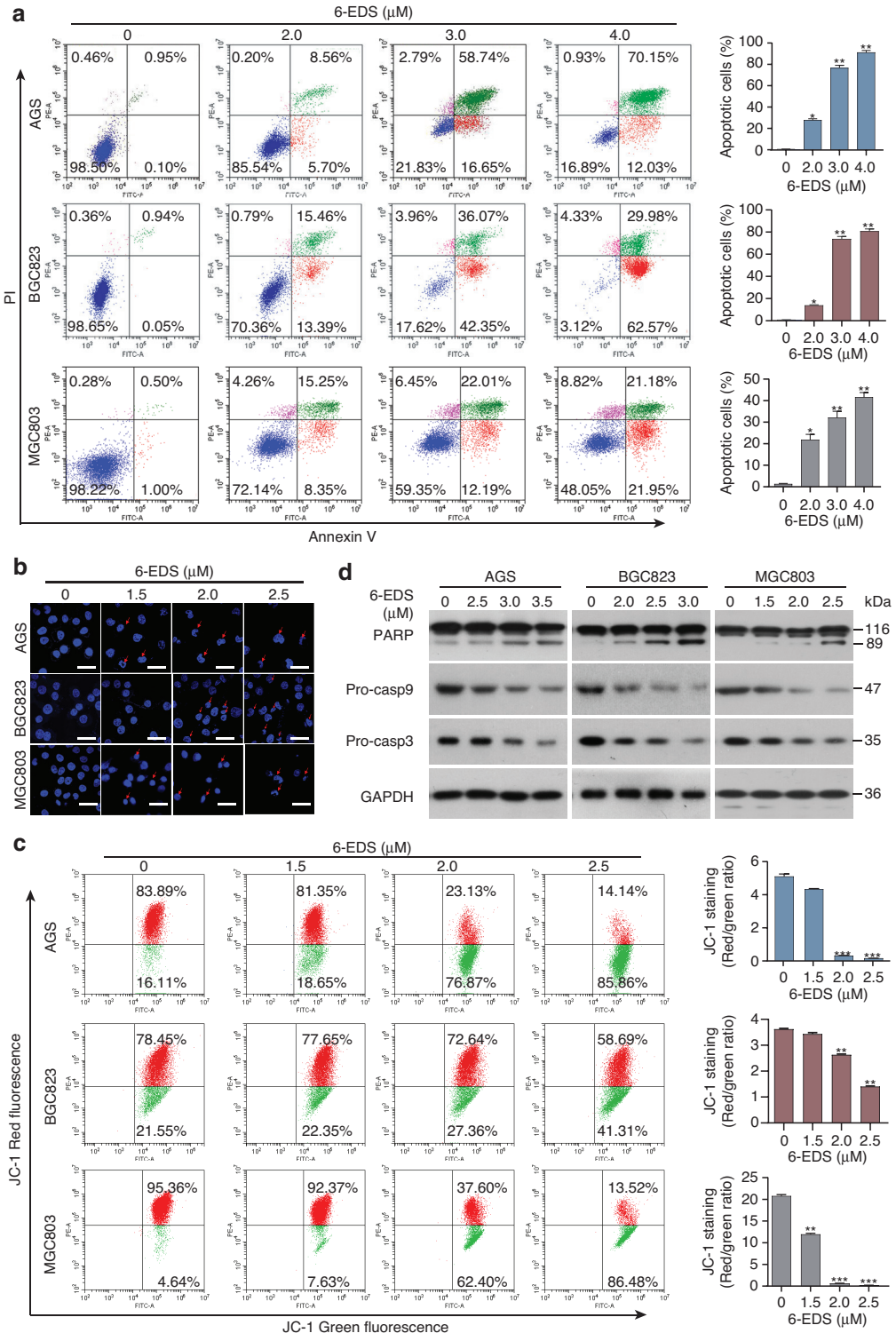

Figure 2 | The compound 6-EDS induces mitochondrially mediated apoptosis in GC cells.
(a) AGS, BGC823, and MGC803 cells were treated with 6-EDS for 24 h and then detected by annexin V/PI staining and flow cytometry. (b) AGS, BGC823, and MGC803 cells were incubated with 6-EDS for 24 h and then examined by DAPI staining. Red arrows indicate apoptotic cells. (c) AGS, BGC823, and MGC803 cells were incubated with 6-EDS for 24 h, and the cell MMP was detected by JC-1 staining and flow cytometry. (d) AGS, BGC823, and MGC803 cells were treated with 6-EDS for 24 h, and western blotting was then performed. *$P < 0.05$, **$P < 0.01$, ***$P < 0.001$.

detected by western blotting, thus indicating that 6-EDS induced a decrease in the precursor form of caspase-3 (pro-casp3) and caspase-9 (pro-casp9), and induced cleavage of PARP in AGS, BGC823, and MGC803 cells (Figure 2d). These data suggested that 6-EDS induced mitochondrially mediated intrinsic apoptosis in GC cells.

3.3 The migratory and invasive behavior of GC cells is suppressed by 6-EDS

High-content imaging technology was used to track the movement of AGS, BGC823, and MGC803 cells. The cell migration and displacement area decreased significantly with increasing 6-EDS concentration (Figure 3a). Wound-healing and Transwell assays were also performed to measure the migratory ability. The 6-EDS treatment significantly inhibited the migration of AGS, BGC823, and MGC803 cells (Figure 3b, 3c). Next, we used RTCA assays to monitor real-time changes in cell invasion by examining the cell index. Under increasing 6-EDS concentrations, the cell-invasion curve decreased significantly (Figure 3d). In Transwell invasion assays, 6-EDS treatment significantly decreased the number of invasive cells (Figure 3e). Therefore, 6-EDS significantly decreased the metastatic ability of GC cells.

3.4 GC progression is suppressed by 6-EDS through inhibition of STAT3 activity

The mechanism of 6-EDS in inhibiting the malignant progression of GC was further investigated. Western blotting analysis indicated that 6-EDS down-regulated the expression of several proteins associated with cell malignant proliferation, migration and invasion, and anti-apoptosis, including cyclin D1, c-Myc, MMP2, MMP9, and survivin (Figure 4a). Moreover, 6-EDS reversed the EMT of GC cells, as manifested primarily in the down-regulation of vimentin and the up-regulation of E-cadherin expression (Figure 4a). Furthermore, qPCR revealed that 6-EDS inhibited the mRNA levels of *MMP2*, *vimentin, c-Myc*, and *cyclin D1* (Figure 4b). These four genes share a common upstream transcription factor, STAT3 [36]. Therefore, we investigated the expression and activation of STAT3. The results suggested that 6-EDS significantly decreased the phosphorylation of Y705 of STAT3, but did not alter the phosphorylation of S727 or the total protein expression level of STAT3 (Figure 4c). Moreover, the expression and phosphorylation of JAK2, a direct regulatory molecule upstream of STAT3, was not affected by 6-EDS (Figure 4c), thus suggesting that 6-EDS may directly suppress the activation of STAT3. The transcriptional activity of STAT3 was further detected by nucleocytoplasmic separation, and 6-EDS was found to inhibit the levels of phosphorylated STAT3 in the nucleus and cytoplasm (Figure 4d). Cytokines and growth factors (e.g., IL-6 and EGF) promote the phosphorylation and activation of STAT3 through their receptors (gp130 and EGFR), thereby promoting the malignant progression of tumors [6]. Further experiments indicated that exogenous IL-6 stimulation promoted STAT3 activation in GC cells, whereas pretreatment with 6-EDS overcame the effects of IL-6 (Figure 4e, 4f). Moreover, 6-EDS overcame the promoting effect of IL-6 on the expression of STAT3 target genes (cyclin D1, c-Myc, and vimentin) (Figure 4e). Although 6-EDS had little effect on EGF-stimulated phosphorylation of EGFR (Figure 4g), this treatment overcame the activation effect of EGF on STAT3, and further decreased the EGF-mediated promotion of the expression of cyclin D1, c-Myc, and vimentin (Figure 4g). These data demonstrated that 6-EDS inhibited the expression of downstream target genes associated with tumor malignant progression by inhibiting STAT3 activity. Next, we determined whether the sensitivity of cells to 6-EDS cytotoxicity was associated with the level of STAT3 expression. GC cells were transfected with the EGFP-STAT3-Myc expression plasmid (Figure 4h). Overexpression of STAT3 significantly antagonized the inhibitory effects of 6-EDS on GC cell proliferation, migration, and invasion (Figure 4i, 4j). Together, the above results suggested that 6-EDS inhibited the malignant progression of GC by directly inhibiting the activity of STAT3.

3.5 The compound 6-EDS directly binds and inhibits STAT3

We further investigated the above *in vitro* results *in silico*. The protein structure of STAT3 is shown in Figure 5a. Molecular docking suggested that 6-EDS binds the SH2 domain of the STAT3-DNA complex (Figure 5b, 5c), and several water molecules mediate the binding of 6-EDS to STAT3. Two water molecules form water bridges between the side chain of K591 and the oxethyl group of 6-EDS. One water mediates the binding of S611 and S613 with the 1,3-benzodioxole of 6-EDS via a water bridge. Another 1,3-benzodioxole group forms a hydrogen bond with the side chain of R609. Hydrophobic interactions occur between the nitrogen methyl group of 6-EDS and the side chains of residues V637 and P639 (Figure 5d). The binding energy of 6-EDS to STAT3 is –6.8 kcal/mol. Next, we performed MD simulations on the 6-EDS–STAT3 complex. The root-mean-square deviation was used to explore the effects of 6-EDS on the binding stability of STAT3 protein. No significant structural differences were observed in short-term simulations. The four systems showed similar trends in RMSD of the protein skeleton, and their average values of RMSD maintained approximately 0.45 nm in the second half of the simulation (Figure 5e). Although previous studies have shown that STAT3 binds DNA only after phosphorylation, recent studies have reported that unphosphorylated STAT3 can also bind DNA [37]. Next, the structural alignment showed that phosphorylated STAT3 and unphosphorylated STAT3 are structurally very similar, except for Y705 (Figure 5f). We additionally estimated the effects of 6-EDS on the DNA binding of STAT3. As shown in Table 2, ΔG_{bind} indicated that unphosphorylated STAT3 (wt-STAT3_DNA) and phosphorylated STAT3 (Y2P-STAT3_DNA) bind DNA with similar energies.

Acta Materia Medica

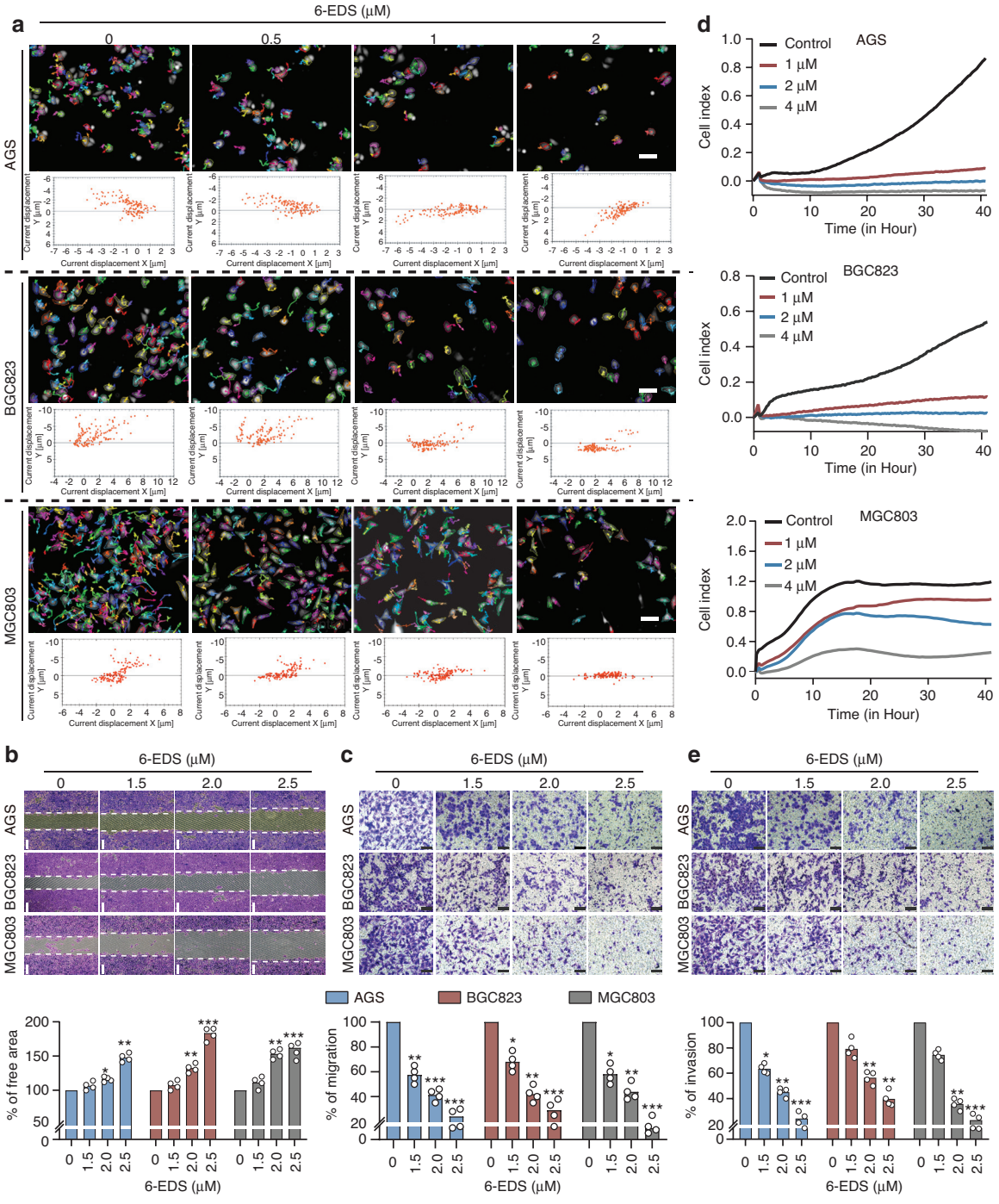

Figure 3 | The compound 6-EDS suppresses the invasive behavior of GC cells.

(a) The movement of AGS, BGC823, and MGC803 cells was analyzed in real time with an Operetta CLS high-content analysis system. After treatment with 6-EDS for 24 h, the cells were imaged with a 20× objective in the DPC channel. Upper panel: Cells were identified with the Find Cells module, and migration was monitored for 12 h with the Track Objects module. Lower panel: Cell displacement was visualized. The current displacement Y was plotted against the current displacement X by using the Multiple Graphs module for display. Each point corresponds to the displacement of a cell at a given time point. Scale bars, 50 μm. (b) Wound-healing assays, performed in 6-EDS-treated AGS, BGC823, and MGC803 cells. Scale bars, 100 μm. (c) Transwell migration assays, performed in 6-EDS-treated AGS, BGC823, and MGC803 cells. Scale bars, 50 μm. (d) AGS, BGC823, and MGC803 cells were cultured in 16-well CIM plates precoated with 250 μg/mL Matrigel for 10–40 h. The invasive ability of the cells was determined by RTCA impedance sensing. The cell index directly correlates with the invasion ability of cells. (e) Transwell invasion assays, performed in 6-EDS-treated AGS, BGC823, and MGC803 cells. Scale bars, 50 μm. $^{*}P < 0.05$, $^{**}P < 0.01$, $^{***}P < 0.001$.

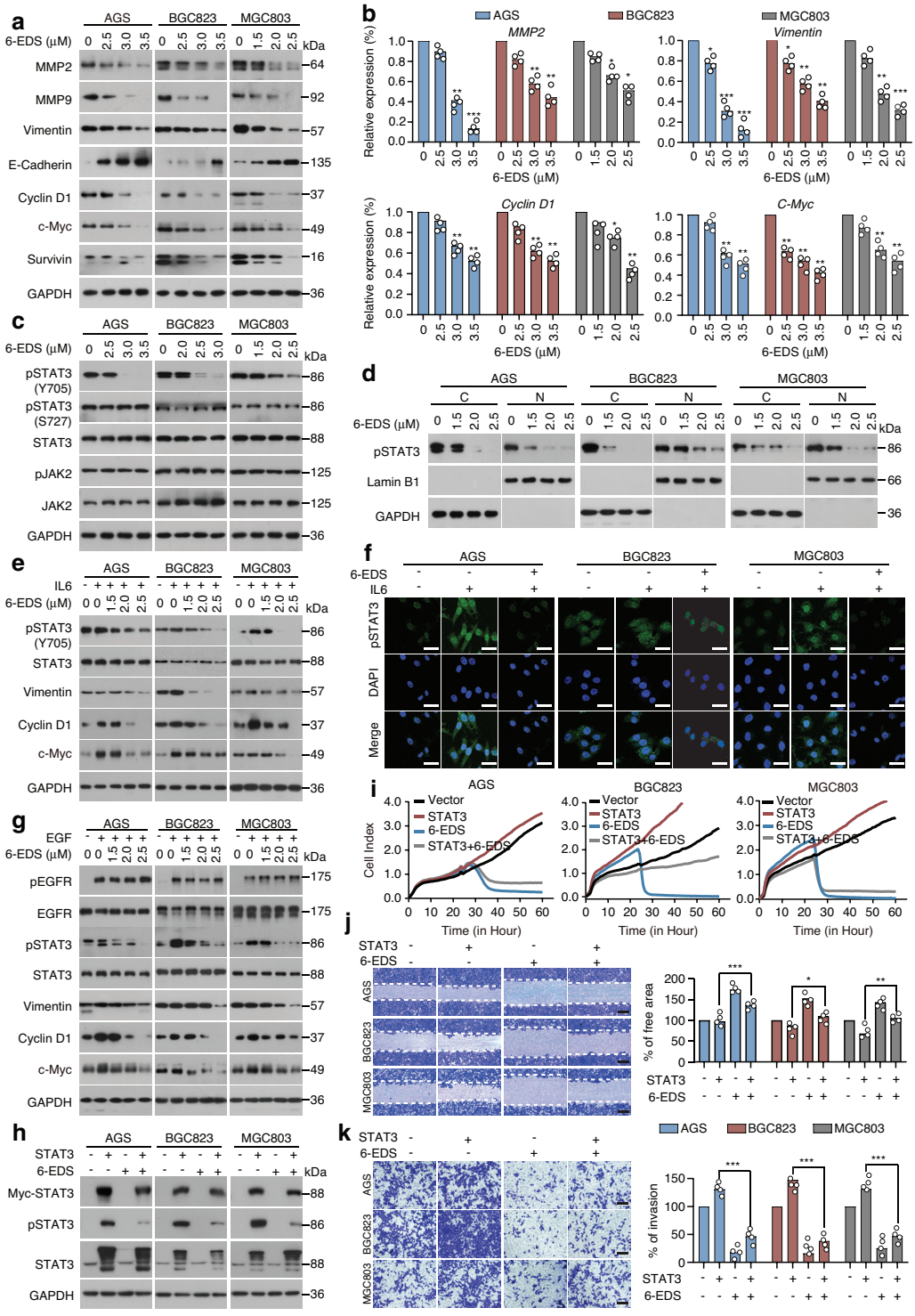

Figure 4 | The compound 6-EDS suppresses GC progression by inhibiting STAT3 activity.
(a–c) AGS, BGC823, and MGC803 cells were treated with 6-EDS for 24 h, and then western blotting or qPCR was performed. (d) AGS, BGC823, and MGC803 cells were treated with 6-EDS for 24 h. The cytoplasmic and nuclear fractions of cells were isolated, and then western blotting was performed. (e–g) AGS, BGC823, or MGC803 cells were pretreated with 6-EDS for 24 h, then stimulated with IL-6 (10 ng/mL) for 10 min or with EGF (100 ng/mL) for 10 min. Western blotting or immunofluorescence assays were used to detect the indicated antibodies. Scale bars, 20 μm. (h–k) AGS, BGC823, or MGC803 cells were transfected with EGFP-STAT3-Myc plasmid, then treated with 6-EDS for 24 h. Western blotting, RTCA, wound-healing, or Transwell invasion assays were used to detect protein expression, cell viability, migration, and invasion. Scale bars, 100 μm (J); 50 μm (k). *P < 0.05, **P < 0.01, ***P < 0.001.

Acta
Materia
Medica

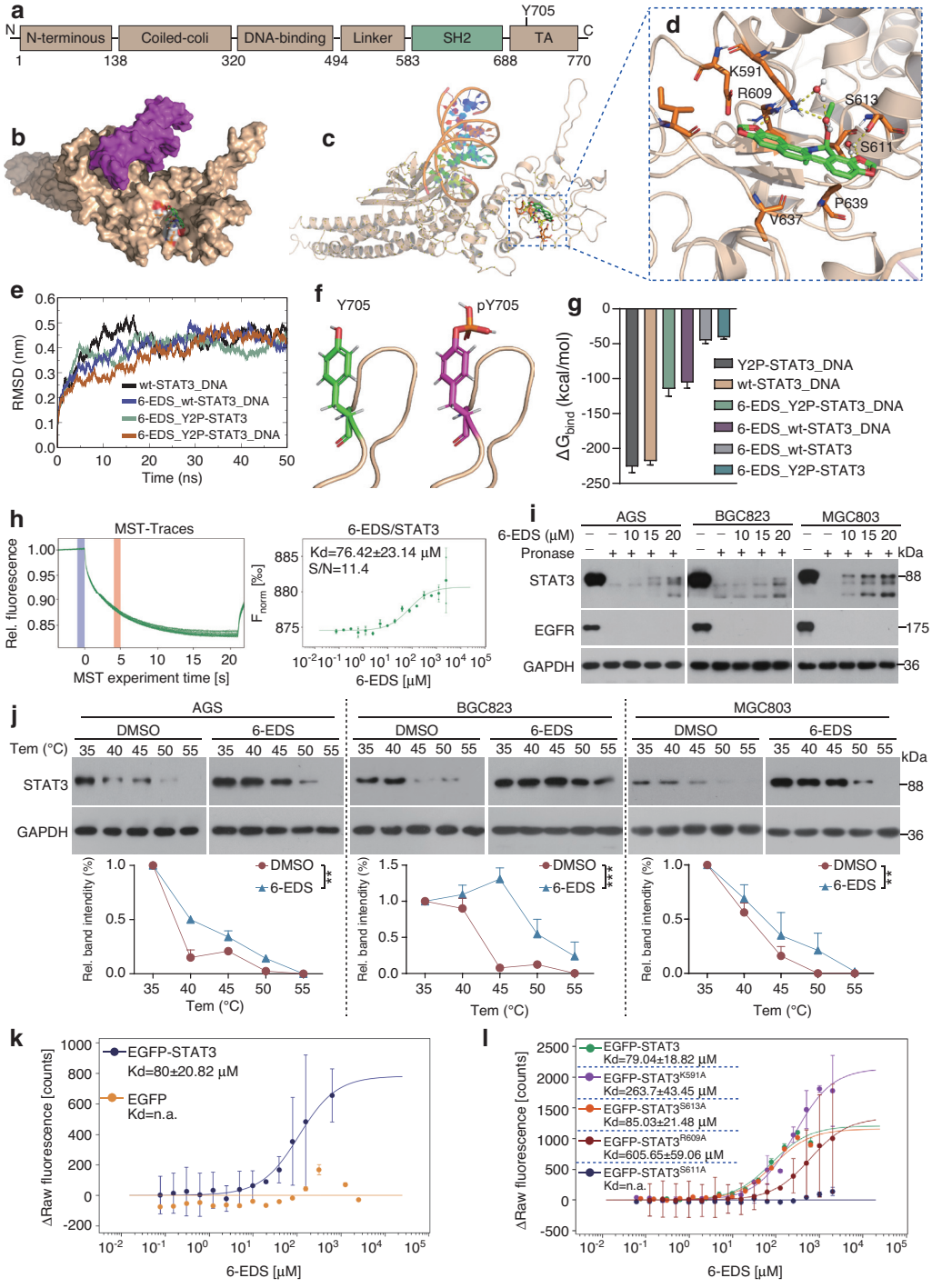

Figure 5 | The compound 6-EDS is an inhibitor that directly binds STAT3.

(a) The domains and boundaries of the domains of STAT3 protein. (b,c) *In silico* molecular docking analysis of 6-EDS with STAT3. (d) Zoomed-in view of 6-EDS at the SH2 domain of STAT3. (e) Root-mean-square-deviation plot of four systems during 50-ns dynamic simulation. (f) The difference between Y705 phosphorylated STAT3 (magenta sticks) and unphosphorylated STAT3 (green sticks). The phosphate group is shown as orange-red sticks. (g) ΔG_{bind} of five systems during energy calculation. (h) Binding affinity of 6-EDS with purified protein, detected with MST assays. (i) Total protein in AGS, BGC823, or MGC803 cells was incubated with different concentrations of 6-EDS, and then treated with pronase to detect the expression of STAT3. (j) AGS, BGC823, or MGC803 cells were treated with 100 μM 6-EDS or DMSO. CETSA was performed to detect the stabilizing effect of 6-EDS on the STAT3 protein. (k, l) HEK293T cells were transfected with EGFP, EGFP-STAT3, EGFP-STAT3^{K591A}, EGFP-STAT3^{R609A}, EGFP-STAT3^{S611A}, or EGFP-STAT3^{S613A} plasmids, and total protein was extracted and then incubated with different concentrations of 6-EDS. MST assays were used to detect the binding affinity. $^{**}P < 0.01$; $^{***}P < 0.001$.

Table 2 | MM/GBSA binding free energy (kcal/mol) of simulation systems.

Energy component	Systems					
	wt-STAT3_DNA	Y2P-STAT3_DNA	6-EDS_wt-STAT3	6-EDS_Y2P-STAT3	6-EDS_wt-STAT3_DNA	6-EDS_Y2P-STAT3_DNA
ΔE_{vdw}	–63.86 ± 4.44	–66.19 ± 14.26	–40.10 ± 3.30	–29.81 ± 3.60	–46.14 ± 4.81	–35.55 ± 7.94
ΔE_{ele}	–1035.82 ± 96.01	–1270.16 ± 111.34	–18.06 ± 7.89	–15.96 ± 3.77	–1270.52 ± 76.17	–890.26 ± 87.68
ΔE_{GB}	890.92 ± 94.95	1119.66 ± 106.10	19.23 ± 5.46	8.77 ± 3.93	1219.46 ± 71.51	816.27 ± 87.97
ΔE_{SURF}	–9.08 ± 0.47	–8.99 ± 1.92	–5.04 ± 0.30	–3.48 ± 0.45	–7.16 ± 0.46	–5.06 ± 1.23
ΔG_{GAS}	–1099.69 ± 96.42	–1336.34 ± 103.66	–59.17 ± 8.84	–45.77 ± 5.51	–916.66 ± 76.46	–925.78 ± 92.47
ΔG_{solv}	881.83 ± 94.97	1110.68 ± 107.01	14.19 ± 5.32	5.28 ± 3.79	811.31 ± 71.31	811.21 ± 81.27
ΔG_{bind}	–217.85 ± 5.81	–225.66 ± 9.00	–44.98 ± 4.63	–40.49 ± 3.00	–105.36 ± 8.19	–114.57 ± 10.55

Interestingly, after 6-EDS binding, the binding energy of DNA with both systems decreased. The binding energy of phosphorylated STAT3 with DNA decreased from –225.66 to –114.57 kcal/mol. The binding energy of unphosphorylated STAT3 with DNA decreased from –217.85 to –105.36 kcal/mol (Figure 5g). These results indicated that the binding of 6-EDS indeed affects the binding ability of phosphorylated or unphosphorylated STAT3 and DNA. From the viewpoint of energy decomposition, the binding of 6-EDS mainly affects the van der Waals interactions and electrostatic interactions between STAT3 and 6-EDS. Collectively, *in silico* validation through dynamics simulations of the docked drug-target complex confirmed the *in vitro* results of the effective inhibition of STAT3 by 6-EDS.

To validate the interaction between 6-EDS and STAT3, and to quantify the binding affinity, we performed microscale thermophoresis (MST) assays. The MST quantification analysis revealed the binding ability of 6-EDS and STAT3 with a K_d of 76.42 μM and a signal-to-noise ratio of 11.4 (Figure 5h). The binding of small molecules promotes the stability of the target protein. Drug-affinity-responsive-target stability assays were conducted to detect the stability of STAT3. Incubation with 6-EDS led to a concentration-dependent decrease in STAT3 proteolysis (Figure 5i). Cellular thermal-shift assays (CETSAs), performed to further confirm the effect of 6-EDS on STAT3 stability, indicated that 6-EDS facilitated STAT3 thermotolerance in a temperature gradient (35–55°C) (Figure 5j). Collectively, these data demonstrated that 6-EDS directly bound STAT3. To further confirm the critical amino acid residues involved in STAT3 binding to 6-EDS, we performed site-directed mutagenesis affecting the K591, R609, S611, and S613 residues in the EGFP-STAT3 plasmid, according to the molecular docking prediction. The EGFP, EGFP-STAT3, EGFP-STAT3^{K591A}, EGFP-STAT3^{R609A}, EGFP-STAT3^{S611A}, and EGFP-STAT3^{S613A} plasmids were transfected into HEK293T cells, and the total protein was extracted and incubated with 6-EDS. MST assays indicated that EGFP-STAT3 bound 6-EDS, whereas EGFP did not (Figure 5k). In addition, the K591A, R609A, S613A mutations had no significant effects on the binding of STAT3 and 6-EDS. K591A and R609A of STAT3 still bound 6-EDS, but the K_d of binding increased significantly, thus indicating a weakened binding effect. In contrast, the S611A mutation inhibited the binding of STAT3 to 6-EDS, thereby suggesting that S611 plays a key role in the binding of STAT3 to 6-EDS. Conclusively, the above results indicated that 6-EDS suppresses the activity of STAT3 and its binding DNA by directly binding the SH2 domain.

3.6 The compound 6-EDS hinders tumor growth *in vivo*

We next detected the inhibitory effect of 6-EDS on tumor growth *in vivo.* After generation of BGC823 murine xenograft models, 6-EDS (2 mg/kg, *i.p.*) was administered for 4 weeks. Subsequently, the mice were sacrificed (Figure 6a). In agreement with the *in vitro* proliferation data, 6-EDS significantly inhibited the of tumor growth *in vivo* (Figure 6b–e). As shown in Figure 6f, treatment with 6-EDS did not cause clear changes in the weights of mice. Diminished Ki67 intensity was observed in the 6-EDS-treated xenograft tumors, as demonstrated by immunohistochemical staining (Figure 6g). In addition, fluorescence immunohistochemistry and western blotting suggested that 6-EDS inhibited the phosphorylation of STAT3 (Figure 6h, 6i). Furthermore, the expression of target genes downstream of STAT3 associated with proliferation, invasion, and migration in tumor tissue was detected by qPCR, thus indicating that 6-EDS significantly decreased the mRNA expression of *MMP2*, *vimentin, cyclin D1*, and *c-Myc* in tumor tissue (Figure 6j). The above results suggested that 6-EDS inhibited tumor progression *in vivo* through STAT3.

Overall, we concluded that 6-EDS inhibits the malignant progression of GC mainly by directly binding the SH2 domain of STAT3, thus inhibiting the phosphorylation and transcriptional activity of STAT3.

4. DISCUSSION

The critical role of STAT3 in malignant tumorigenesis and progression has sparked research in targeted drug

Acta Materia Medica

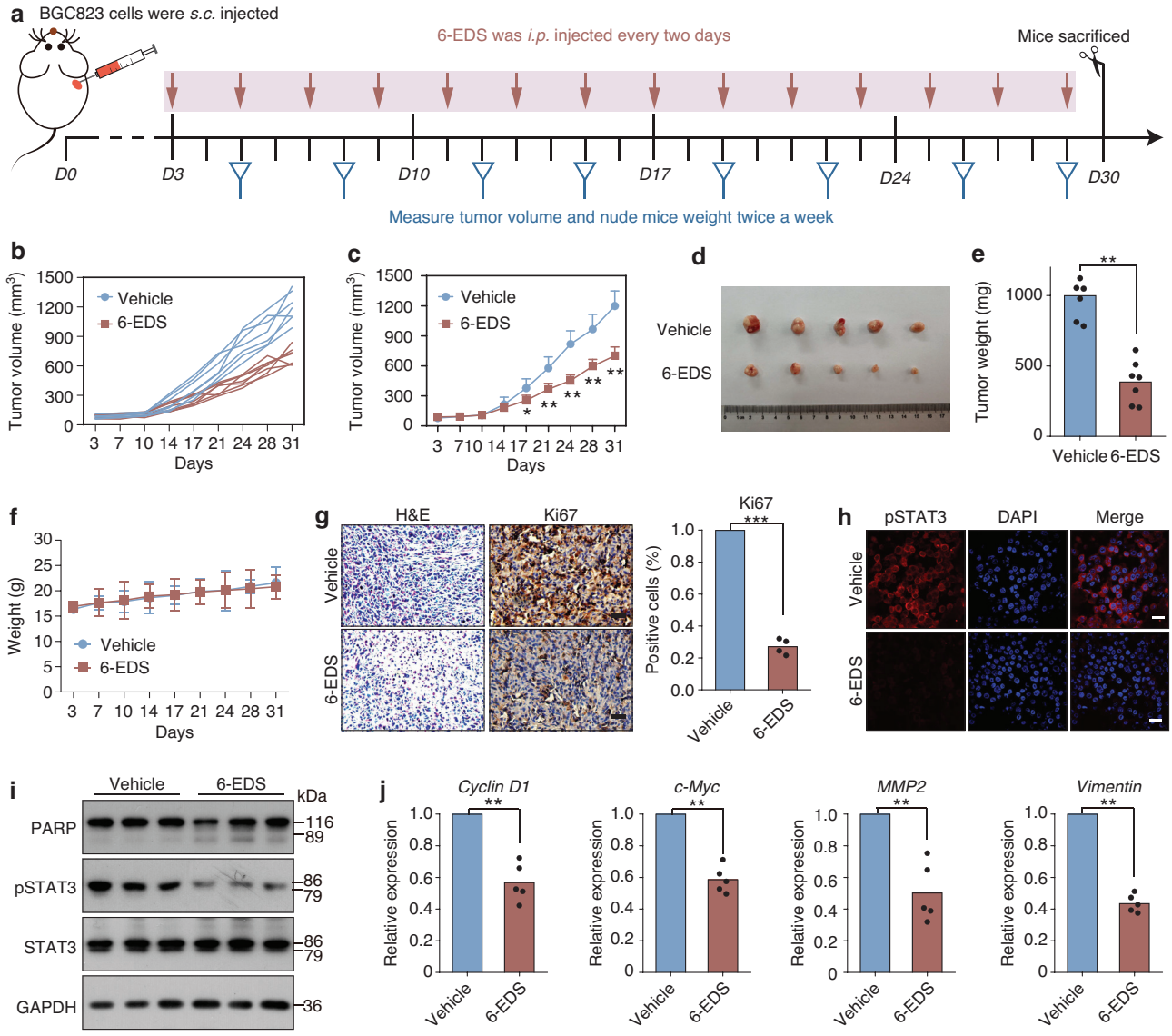

Figure 6 | The compound 6-EDS hinders tumor growth *in vivo*.
(a) Process diagram of xenograft tumor models. (b, c) Tumor volumes of nude mice after 2 mg/kg 6-EDS treatments. (d) Images of xenograft tumors obtained from the sacrificed mice. (e) Weights of the tumors from the sacrificed mice. (f) Body weights of nude mice after 6-EDS treatments. (g) H&E staining and immunohistochemistry staining of representative tumor tissues. Scale bars, 50 μm. (h) Immunofluorescence staining of representative tumor tissues. Scale bars, 20 μm. (i) Western blot assays of representative tumor tissues. (j) qPCR detection of representative tumor tissues. $^{*}P < 0.05$, $^{**}P < 0.01$, $^{***}P < 0.001$.

discovery to screen small molecules that perturb STAT3 activity. Here, we examined a novel small-molecule STAT3 inhibitor, 6-EDS, which has shown great promise in pre-clinical evaluations of GC treatment. We observed clear toxicity effects of 6-EDS on GC cell survival, including promoting cell apoptosis, and decreasing invasion and migration. Moreover, 6-EDS decreased tumor burden in GC xenografts *in vivo*. These anti-tumor effects were exerted by 6-EDS binding the SH2 domain, and inhibiting the binding of phosphorylated and non-phosphorylated STAT3 to DNA.

We further demonstrated that 6-EDS inhibited GC cell viability and induced GC cell apoptosis by affecting the mitochondrial apoptosis pathway mediated by caspase-9. The down-regulation of the pro-survival molecule survivin downstream of STAT3 by 6-EDS may be involved in the activation of the above apoptotic signals [38]. We used RTCA and a high-content imaging system to demonstrate that 6-EDS significantly inhibited the viability, area, and motility of GC cells. Increased cell roundness indicates decreased cellular activity and migratory ability [39]. Various cytokines, growth factors,

and intracellular signaling pathways promote tumor cell survival and malignant progression by activating STAT3 signaling [10]. We detected IL-6 and EGF signaling upstream of STAT3 and the key regulatory molecule JAK2, thus demonstrating that 6-EDS down-regulated the expression of downstream target genes associated with invasion, migration, and EMT by directly inhibiting STAT3 activity. Knockdown of STAT3 has been widely reported to significantly inhibit GC cell growth, EMT, and consequent tumor invasion and migration [40, 41]. Our investigation further demonstrated that overexpression of STAT3 significantly antagonized the inhibitory effect of 6-EDS on GC cell malignant progression, thus suggesting that 6-EDS inhibits GC malignant progression at least partly by inhibiting STAT3.

Currently, the core strategies for targeting STAT3 include suppressing STAT3 phosphorylation, binding the SH2 domain, disrupting STAT3-DNA binding, or suppressing STAT3 transcriptional activity [42]. Targeting the SH2 domain is the main method to screen for STAT3 inhibitors, but targeting the SH2 domain to inhibit STAT3 phosphorylation and dimerization may not completely inhibit abnormal STAT3 signal transduction. Recently, studies have reported that STAT3 participates in transcriptional regulation without tyrosine phosphorylation; that is, non-phosphorylated STAT3 dimers bind DNA and promote transcription [43, 44]. Inhibition of phosphorylated and non-phosphorylated STAT3 binding DNA may represent another effective method to eliminate STAT3 signaling. Molecular docking analysis showed that the best docking orientation for 6-EDS binding STAT3 was the SH2 domain. The 6-EDS bound the SH2 domain and inhibited the phosphorylation of Y705, thereby repressing STAT3 dimerization. The dimerization region of STAT3 covers the SH2 domain and the 688–722 aa region of the transactivation domain, where Y705 resides. The phosphorylation of Y705 is necessary for dimerization [42]. Binding of 6-EDS decreased the dimerization and nuclear entry of STAT3, and may also be detrimental to the phosphorylation of STAT3 through structural changes. The energy dissipation-cum-signaling mechanism suggests that local structural changes or binding ligands are thermodynamically coupled to the distal activation site [45]. The conformational changes caused by mutation or ligand binding can be 20 Å or more, thus resulting in identifiable functional consequences on kinase activity [46]. The binding of 6-EDS in the SH2 domain may be thermodynamically coupled to the Y705 site through distal residues, thereby affecting the degree of phosphorylation of Y705. Moreover, MD simulations indicated that, although 6-EDS did not bind the DNA binding domain, it decreased the binding free energy of phosphorylated STAT3 and non-phosphorylated STAT3 to target gene DNA. Binding free energy is dominated by electrostatic and hydrophobic interactions. Moreover, 6-EDS has strong electronegativity and thus binds basic amino acids, such as K591 and R609. With the participation of water molecules, the side chain of S611 formed a hydrogen bond with 6-EDS. As a polar hydrophilic amino acid, S611 has no other interactions, an aspect potentially important in recognizing intermolecular binding. Furthermore, we demonstrated the direct binding effect of 6-EDS and STAT3 and key amino acid sites through MST, CETSA, and drug-affinity-responsive-target stability assays. Although site-directed mutagenesis indicated that the S611 site of STAT3 played a critical role in binding 6-EDS, the affinity of 6-EDS toward the STAT3 protein must be further improved.

Conclusively, our data reveal that 6-EDS is a novel STAT3 inhibitor, and demonstrate that 6-EDS has a significant inhibitory effect on the survival, invasion, and migration of GC cells, and activates mitochondrial apoptosis. These effects are associated with direct inhibition of STAT3 by 6-EDS. This study may provide an experimental foundation for antitumor targeted therapy based on 6-EDS.

ACKNOWLEDGEMENTS

This work was supported by grants from the National Natural Science Foundation of China (No. 82203409); the Foundation for the Innovative Research Group of the Hubei Provincial Department of Science and Technology (no. 2021CFA009); the Principal Investigator grant of Hubei University of Medicine (no. HBMUPI201806); the Advantages Discipline Group Project in Higher Education of Hubei Province (2021–2025) (no. 2022XKQT2); the Open Project from the Zhejiang Provincial Key Laboratory of Cancer Molecular Cell Biology, Life Sciences Institute, Zhejiang University; the Scientific and Technological Project of Shiyan City of Hubei Province (no. 21Y09); and the National Training Program of Innovation and Entrepreneurship for Undergraduates (no. 202210929009).

CONFLICTS OF INTEREST

The authors declare no conflicts of interest.

REFERENCES

[1] Sung H, Ferlay J, Siegel RL, Laversanne M, Soerjomataram I, Jemal A, et al.: Global Cancer Statistics 2020: GLOBOCAN Estimates of Incidence and Mortality Worldwide for 36 Cancers in 185 Countries. *CA: A Cancer Journal for Clinicians* 2021, 71:209–249.

[2] Chen W, Zheng R, Baade PD, Zhang S, Zeng H, Bray F, et al.: Cancer Statistics in China, 2015. *CA: A Cancer Journal for Clinicians* 2016, 66:115–132.

[3] Kurumi H, Nonaka K, Ikebuchi Y, Yoshida A, Kawaguchi K, Yashima K, et al.: Fundamentals, Diagnostic Capabilities and Perspective of Narrow Band Imaging for Early Gastric Cancer. *Journal of Clinical Medicine* 2021, 10:2918.

[4] Mocan L: Surgical Management of Gastric Cancer: A Systematic Review. *Journal of Clinical Medicine* 2021, 10:2557.

[5] Tolomeo M, Cascio A: The Multifaced Role of STAT3 in Cancer and Its Implication for Anticancer Therapy. *International Journal of Molecular Sciences* 2021, 22:603.

[6] Zou S, Tong Q, Liu B, Huang W, Tian Y, Fu X: Targeting STAT3 in Cancer Immunotherapy. *Molecular Cancer* 2020, 19:145.
[7] Johnson DE, O'Keefe RA, Grandis JR: Targeting the IL-6/JAK/STAT3 Signalling Axis in Cancer. *Nature Reviews Clinical Oncology* 2018, 15:234–248.
[8] Frank DA: STAT3 as a Central Mediator of Neoplastic Cellular Transformation. *Cancer Letters* 2007, 251:199–210.
[9] Roeser JC, Leach SD, McAllister F: Emerging Strategies for Cancer Immunoprevention. *Oncogene* 2015, 34:6029–6039.
[10] Thilakasiri PS, Dmello RS, Nero TL, Parker MW, Ernst M, Chand AL: Repurposing of Drugs as STAT3 Inhibitors for Cancer Therapy. *Seminars in Cancer Biology* 2021, 68:31–46.
[11] Lee M, Hirpara JL, Eu JQ, Sethi G, Wang L, Goh BC, et al.: Targeting STAT3 and Oxidative Phosphorylation in Oncogene-Addicted Tumors. *Redox Biology* 2019, 25:101073.
[12] Villarino AV, Kanno Y, O'Shea JJ: Mechanisms and Consequences of Jak-STAT Signaling in the Immune System. *Nature Immunology* 2017, 18:374–384.
[13] Huang P, Xia L, Liu W, Jiang R, Liu X, Tang Q, et al.: Hairy Root Induction and Benzylisoquinoline Alkaloid Production in Macleaya Cordata. *Scientific Reports* 2018, 8:11986.
[14] Psotová J, Klejdus B, Vecera R, Kosina P, Kubán V, Vicar J, et al.: A Liquid Chromatographic-mass Spectrometric Evidence of Dihydrosanguinarine as a First Metabolite of Sanguinarine Transformation in Rat. *Journal of Chromatography B Analytical Technologies in the Biomedical and Life Sciences* 2006, 830:165–172.
[15] Kosina P, Gregorova J, Gruz J, Vacek J, Kolar M, Vogel M, et al.: Phytochemical and Antimicrobial Characterization of Macleaya Cordata Herb. *Fitoterapia* 2010, 81:1006–1012.
[16] Ouyang L, Su XL, He DS, Chen YY, Ma M, Xie QJ, et al.: A Study on Separation and Extraction of Four Main Alkaloids in Macleaya Cordata (Willd) R. Br. with Strip Dispersion Hybrid Liquid Membrane. *Journal of Separation Science* 2010, 33:2026–2034.
[17] Yao JY, Shen JY, Li XL, Xu Y, Hao GJ, Pan XY, et al.: Effect of Sanguinarine from the Leaves of Macleaya Cordata Against Lchthyophthirius Multifiliis in Grass Carp (Ctenopharyngodon idella). *Parasitology Research* 2010, 107:1035–1042.
[18] Ni H, Martinez Y, Guan G, Rodriguez R, Mas D, Peng H, et al.: Analysis of the Impact of Isoquinoline Alkaloids, Derived from Macleaya cordata Extract, on the Development and Innate Immune Response in Swine and Poultry. *BioMed Research International* 2016, 2016:1352146.
[19] Lin L, Liu YC, Huang JL, Liu XB, Qing ZX, Zeng JG, et al.: Medicinal Plants of the Genus Macleaya (Macleaya Cordata, Macleaya Microcarpa): A Review of Their Phytochemistry, Pharmacology, and Toxicology. *Phytotherapy Research: PTR* 2018, 32:19–48.
[20] Konda Y, Urono M, Harigaya Y, Onda M: Studies on the Constituents of Bocconia-Cordata 0.4. Transformation of Sanguinarine into Bocconine. *Journal of Heterocyclic Chemistry* 1991, 28:1841–1843.
[21] Wang J, Wang YJ, Wang ZQ, Wang F, He J, Yang XY, et al.: A Thermosensitive Gel Based on w1/o/w2 Multiple Microemulsions for the Vaginal Delivery of Small Nucleic Acid. *Drug Delivery* 2019, 26:168–178.
[22] Si Y, Wang J, Liu XW, Zhou T, Xiang YC, Zhang T, et al.: Ethoxysanguinarine, a Novel Direct Activator of AMP-Activated Protein Kinase, Induces Autophagy and Exhibits Therapeutic Potential in Breast Cancer Cells. *Frontiers in Pharmacology* 2020, 10:1503.
[23] Ma WJ, Xiang YC, Yang R, Zhang T, Xu JX, Wu YZ, et al.: Cucurbitacin B Induces Inhibitory Effects Via the CIP2A/PP2A/C-KIT Signaling Axis in t(8;21) Acute Myeloid Leukemia. *Journal of Pharmacological Sciences* 2019, 139:304–310.
[24] Xiang YC, Shen J, Si Y, Liu XW, Zhang L, Wen J, et al.: Paris Saponin VII, A Direct Activator of AMPK, Induces Autophagy and Exhibits Therapeutic Potential in Non-Small-Cell Lung Cancer. *Chinese Journal of Natural Medicines* 2021, 19:195–204.
[25] Zhang YF, Huang P, Liu XW, Xiang YC, Zhang T, Wu YZ, et al.: Polyphyllin I Inhibits Growth and Invasion of Cisplatin-Resistant Gastric Cancer Cells by Partially Inhibiting CIP2A/PP2A/Akt Signaling Axis. *Journal of Pharmacological Sciences* 2018, 137:305–312.
[26] Li SX, Olson WK, Lu XJ: Web 3DNA 2.0 for the Analysis, Visualization, and Modeling of 3D Nucleic Acid Structures. *Nucleic Acids Research* 2019, 47: W26–W34.
[27] Chow E, Rendleman CA, Bowers KJ, Dror RO, Hughes DH, Gullingsrud J, et al.: Desmond Performance on a Cluster of Multicore Processors. 2008, DE Shaw Research Technical Report DESRES/TR--2008-01.
[28] Pronk S, Páll S, Schulz R, Larsson P, Bjelkmar P, Apostolov R, et al.: GROMACS 4.5: A High-Throughput and Highly Parallel Open Source Molecular Simulation Toolkit. *Bioinformatics* 2013, 29:845–854.
[29] Hornak V, Abel R, Okur A, Strockbine B, Roitberg A, Simmerling CJPS, Function, et al.: Comparison of Multiple Amber Force Fields and Development of Improved Protein Backbone Parameters. *Proteins: Structure, Function, and Bioinformatics* 2006, 65:712–725.
[30] Wang JM, Wolf RM, Caldwell JW, Kollman PA, Case DA: Development and Testing of a General Amber Force Field. *Journal of Computational Chemistry* 2004, 25: 1157–1174.
[31] Hess B: P-LINCS: A Parallel Linear Constraint Solver for Molecular Simulation. *Journal of Chemical Theory and Computation* 2008, 4:116–122.
[32] Valdés-Tresanco MS, Valdés-Tresanco ME, Valiente PA, Moreno EJ: gmx_MMPBSA: A New Tool to Perform End-State Free Energy Calculations with GROMACS. *Journal of Chemical Theory and Computation* 2021, 17:6281–6291.
[33] Homeyer N, Gohlke H: Free Energy Calculations by the Molecular Mechanics Poisson–Boltzmann Surface Area Method. *Molecular Informatics* 2012, 31:114–122.
[34] Yang T, Wu JC, Yan C, Wang Y, Luo R, Gonzales MB, et al.: Virtual Screening Using Molecular Simulations. *Proteins: Structure, Function, and Bioinformatics* 2011, 79:1940–1951.
[35] Choi J, Lee YJ, Yoon YJ, Kim CH, Park SJ, Kim SY, et al.: Pimozide Suppresses Cancer Cell Migration and Tumor Metastasis Through Binding to ARPC2, A Subunit of the Arp2/3 Complex. *Cancer Science* 2019, 110:3788–3801.
[36] Banerjee K, Resat H: Constitutive Activation of STAT3 in Breast Cancer Cells: A Review. *International Journal of Cancer* 2016, 138:2570–2578.
[37] Nkansah E, Shah R, Collie GW, Parkinson GN, Palmer J, Rahman KM, et al.: Observation of Unphosphorylated STAT3 Core Protein Binding to Target dsDNA by PEMSA

and X-ray Crystallography. *FEBS Letters* 2013, 587: 833–839.

[38] Ahmad B, Gamallat Y, Su P, Husain A, Rehman AU, Zaky MY, et al.: Alantolactone Induces Apoptosis in THP-1 Cells Through STAT3, Survivin Inhibition, and Intrinsic Apoptosis Pathway. *Chemical Biology & Drug Design* 2021, 97:266–272.

[39] Yadav S, Vadivelu R, Ahmed M, Barton M, Nguyen NT: Stretching Cells - An Approach for Early Cancer Diagnosis. *Experimental Cell Research* 2019, 378:191–197.

[40] Sun Y, Guo BF, Xu LB, Zhong JT, Liu ZW, Liang H, et al.: Stat3-siRNA Inhibits the Growth of Gastric Cancer in Vitro and in Vivo. *Cell Biochemistry and Function* 2015, 33:495–502.

[41] Yu J, Zhou ZJ, Wei Z, Wu J, OuYang J, Huang WB, et al.: FYN Promotes Gastric Cancer Metastasis by Activating STAT3-Mediated Epithelial-Mesenchymal Transition. *Translational Oncology* 2020, 13:100841.

[42] Dong J, Cheng XD, Zhang WD, Qin JJ: Recent Update on Development of Small-Molecule STAT3 Inhibitors for Cancer Therapy: From Phosphorylation Inhibition to Protein Degradation. *Journal of Medicinal Chemistry* 2021, 64:8884–8915.

[43] Nishimoto A, Kugimiya N, Hosoyama T, Enoki T, Li TS, Hamano K: JAB1 Regulates Unphosphorylated STAT3 DNA-Binding Activity Through Protein-Protein Interaction in Human Colon Cancer Cells. *Biochemical and Biophysical Research Communications* 2013, 438:513–518.

[44] Timofeeva OA, Chasovskikh S, Lonskaya I, Tarasova NI, Khavrutskii L, Tarasov SG, et al.: Mechanisms of Unphosphorylated STAT3 Transcription Factor Binding to DNA. *Journal of Biological Chemistry* 2012, 287:14192–14200.

[45] Li JZ, Huang Y, Wu MM, Wu CF, Li X, Bao JK: Structure and Energy Based Quantitative Missense Variant Effect Analysis Provides Insights into Drug Resistance Mechanisms of Anaplastic Lymphoma Kinase Mutations. *Scientific Reports* 2018, 8:10664.

[46] Rajasekaran N, Sekhar A, Naganathan AN: A Universal Pattern in the Percolation and Dissipation of Protein Structural Perturbations. *The Journal of Physical Chemistry Letters* 2017, 8:4779–4784.